TEM studies of metal dichloride and metal trichloride graphite intercalation compounds

1990 J. Phys.: Condens. Matter 2 6471

(http://iopscience.iop.org/0953-8984/2/31/001)

J. Phys.: Condens. Matter **2** (1990) 6471–6489. Printed in the UK

TEM studies of metal dichloride and metal trichloride graphite intercalation compounds

J S Speck†§¶ and M S Dresselhaus‡

† Department of Materials Science and Engineering, Massachusetts Institute of Technology, Cambridge, MA 02139, USA

‡ Department of Electrical Engineering and Computer Science and Department of Physics, Massachusetts Institute of Technology, Cambridge, MA 02139, USA

Received 19 February 1990

Abstract. Transmission electron microscopy (TEM) studies have been carried out on stage 1 and stage 2 $CoCl_2$-GIC and $CuCl_2$-GIC. These studies show that the intercalate has crystallographic coherence lengths of the order of 1 μm in the basal plane, whereas the continuity length may be of the order of 200 Å. The structure of $InCl_3$-GIC has also been studied and two new phases have been discovered: a nearly commensurate $\sqrt{7} \times \sqrt{7}$ R19.1° phase believed to be stage 1; and an aligned incommensurate phase believed to be of high stage. The nearly commensurate $\sqrt{7} \times \sqrt{7}$ R19.1° phase displays both crystallographic coherence lengths and continuity lengths of the order of 1 μm.

1. Introduction

The metal dichloride graphite intercalation compounds (GICs) exhibit at least four interesting structural features:

(i) incomplete intercalate coverage of the carbon layer;

(ii) a reported excess of chlorine in the stoichiometry of the compounds;

(iii) three-dimensional ordering of the intercalate and carbon in stage 1 compounds and two-dimensional ordering of the intercalate in stage 2 and higher-stage compounds [1].

(iv) rotational epitaxy of the incommensurate intercalate layers relative to the carbon layers [1].

In this paper we focus on the first two features and discuss the interplay of all four structural features. Additionally, the structure of a commensurate metal trichloride GIC system, $InCl_3$-GIC, will be contrasted with the structure of the metal dichloride GICs.

The incomplete intercalate coverage of the carbon layer for the metal dichloride GICs is more commonly described as the *filling factor*. The filling factor is determined by first measuring the in-plane unit cell parameters of the metal dichloride layer after intercalation either by transmission electron microscopy (TEM) or by x-ray methods. The ideal intercalate density per unit area and the ideal carbon density per unit area lead to the ideal stoichiometric formula for the compound: $C_{yn}MCl_{2+\delta}$ where y is the ideal

§ Email address: speck @ tony. ucsb. edu.

¶ Present address: Materials Department, University of California, Santa Barbara, CA 93106, USA.

0953-8984/90/316471 + 19 $03.50

number of carbon atoms per metal ion for one layer, n is the stage index, and δ is the chlorine excess. The observed stoichiometry is determined by either weight uptake, fits of occupancy factors of the metal cations and chlorine anions in structure factor refinements, or by direct chemical analysis (e.g., wet chemistry, x-ray fluorescence). The filling factor is given as the ratio of the calculated ideal value of y over the observed value y_{obs}. In all cases where filling factors for metal dichloride GICs have been reported in the literature, the observed values have been in the range 0.6 to 0.9 [2, 3].

The non-uniform filling of the intercalate layer in the metal dichloride GICs leads to the question of the actual intercalate *distribution* on a given layer. It has been suggested that the intercalate exists in an islandic form and that there is chlorine segregation to the island boundaries, thereby providing the necessary charge transfer for the intercalation reaction [2, 4]. If it is assumed that all of the peripheral chlorine ions at an island boundary contribute to the charge transfer, then simple calculations predict island sizes in the 100–500 Å range based on the measured chlorine excesses [2, 4]. Island sizes of this order of magnitude have been deduced from the linewidths of x-ray and neutron Bragg peaks [5–8], small-angle neutron scattering measurements [6, 9] and coherence lengths of moiré fringes in dark-field TEM images [6, 9]. Although all of the experimental results on island sizes form a reasonably consistent picture of the structure, none of the reported results thus far unambiguously resolves the question of the intercalate distribution.

Intercalate coherence lengths of the order of 100 Å suggest that TEM is the ideal technique for directly resolving the intercalate distribution. In past studies, thin samples for TEM have been prepared by peeling intercalated pieces of graphite with Scotchtape and then dissolving either the mounting medium for the GIC or the Scotchtape with an appropriate solvent and then mounting the resulting thin section on a TEM grid. Samples prepared in such a fashion almost always give diffraction patterns with a wide arc of intercalate reflections [10]. When the intercalate reflections are used to form the dark-field image, overlapping intercalate layers interfere, leading to complex moiré fringe images and providing little direct information on the intercalate distribution. The drawback in preparing samples by the above methods is that the peeling action of the Scotchtape may inflict substantial damage on the GIC and the further action of solvents may disturb the intercalate structure. Nevertheless, in this paper, we will show that the statistics of selected-area diffraction patterns can be used to infer information about the intercalate distribution in samples prepared by peeling with Scotchtape. Further, in cases where there are a small number of overlapping layers, the length of moiré fringes can be used to determine the minimum crystallographic coherence length in the intercalate layer.

An alternate route to preparing thin samples for TEM is to intercalate graphite powder and directly examine the resulting GIC. In this case, we will show that it is possible to obtain direct information on the distribution of the intercalate in the metal dichloride GICs.

2. Experimental procedure

Single-crystal intercalation compounds were produced by reacting natural flake graphite with either pure $CoCl_2$, $CuCl_2$, or $InCl_3$ in a sealed reaction ampoule with a chlorine overpressure. The exact reaction conditions for preparing the $CoCl_2$-GICs and $CuCl_2$-GICs are given elsewhere [1]. The $InCl_3$-GICs were prepared by reacting the natural

graphite with pure powdered $InCl_3$ in a sealed reaction ampoule. The chlorine overpressure at ambient temperature was 1 atm. The reaction took place for 26 days at 450 °C. Powder samples of stage 1 $CoCl_2$-GIC were prepared by placing natural graphite powder and either pure $CoCl_2$ or pure $CuCl_2$ powder in a sealed reaction ampoule with a chlorine overpressure of $\simeq 3$ atm. The reaction took place for 7 or 14 days at 560 °C. The powder GIC samples were repeatedly cleaned in methyl-ethyl ketone and acetone to remove any excess unreacted $CoCl_2$ or $CuCl_2$.

TEM specimens of the natural flake GICs were prepared by cleaving thin sections of the sample with Scotchtape. The thin sections were removed from the Scotchtape and mounted on either 100-mesh or 200-mesh folding copper grids. The samples were then repeatedly cleaned with acetone and methyl-ethyl ketone. TEM specimens of the powder GIC samples were directly prepared by dipping a carbon-coated copper grid into the GIC powder. The TEM measurements were performed on either a JEOL 200 CX TEM operating at 200 kV or a JEOL 4000 EX TEM operating at 400 kV. STEM measurements were performed on a Vacuum Generators HB-5 instrument.

3. Results and image interpretation

In this section the crystallographic coherence length and continuity length of the intercalate layers of stage 1 and stage 2 MCl_2-GICs are determined by TEM imaging and electron diffraction. Additionally, two new phases are reported for $InCl_3$-GICs.

3.1. Metal–dichloride GICs: Moiré fringes

Experimentally it is difficult to make TEM samples thin enough to resolve individual intercalate domains. Generally, the TEM foils are too thick and as a result there are several different intercalate domains with different orientations which overlap through the thickness of the foil. Each different intercalate orientation represents one sample from the parent rotational epitaxy distribution for the crystal. An example of a diffraction pattern displaying a range of intercalate orientations is shown in figure 1(*a*) for stage 1 $CoCl_2$-GIC. Dark-field images formed with a grouping of intercalate reflections give rise to complex moiré images, as shown in figure 1(*b*). These images are difficult to interpret because information from too many domains is superposed. Such images, until now, represent the state of the art in TEM studies of metal dichloride GICs.

The stage 1 character of the particle used to form the selected-area diffraction pattern and the dark-field image of figure 1 was verified by x-ray precession photographs. Zero-level *c*-axis precession photographs of stage 1 and 2 $CoCl_2$-GICs are shown elsewhere [1]. The rotational epitaxy angle for stage 1 is easily observed to be 0° with a 2.5° spread FWHM as determined by four-circle diffractometry [1]. However, the rotational epitaxy angle for stage 2 is observed to be 30° [1]. Inspection of figure 1 shows that the epitaxy angles agree and the particle used for imaging in figure 1 is indeed stage 1. Inspection of figure 1(*a*) shows the range of orientations that the intercalate layer can possess, through the arcing of the intercalate spots.

In some cases it is possible to find regions that are sufficiently thin to have only two or three different intercalate domains overlaying. In powder samples it is possible to find such thin particles (see figure 2(*a*)) which have repeatedly cleaved under the frictional forces resulting from dipping the carbon film into the intercalated graphite powder. The diffraction pattern from one of these particles, figure 2(*b*), is identified as

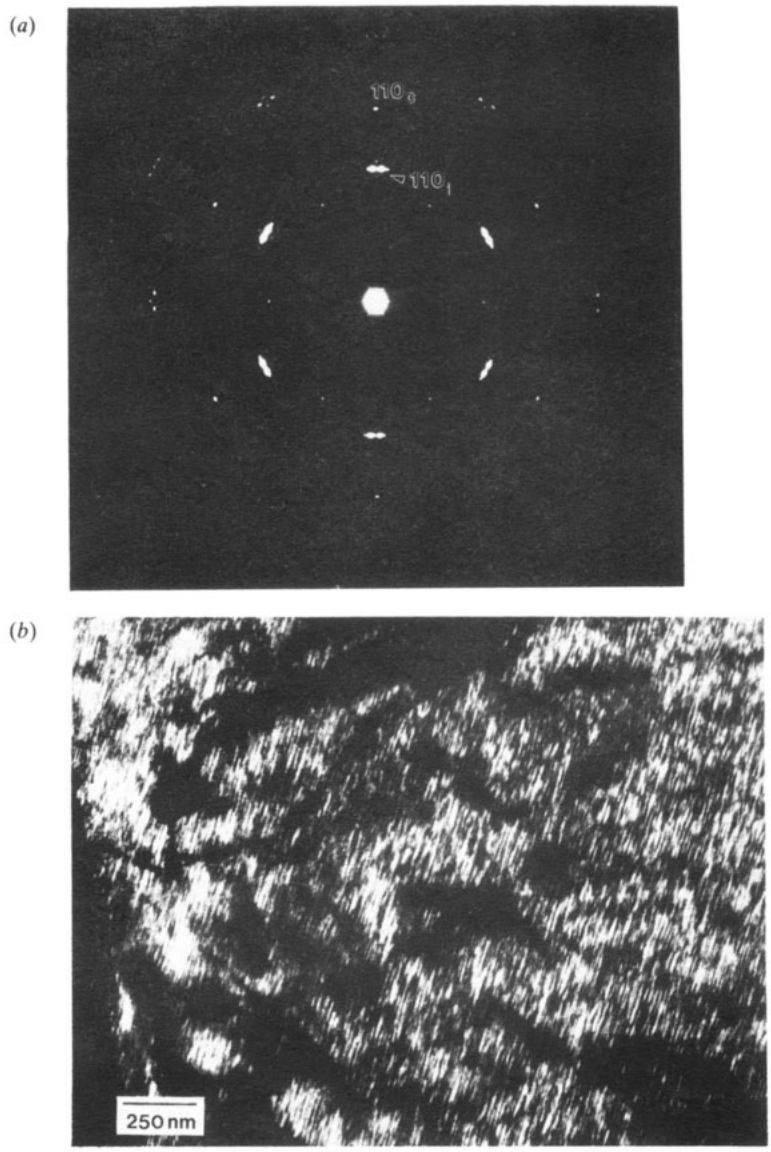

Figure 1. (*a*) Selected-area electron diffraction pattern from stage 1 $CoCl_2$-GIC—note the angular distribution of $CoCl_2$ reflections. (*b*) Dark-field image formed using 110_{CoCl_2}. Note the complicated moiré fringe pattern.

stage 2 or higher stage because of the 30° rotation between the intercalate and carbon lattices. In this case there are two overlaying intercalate domains. The 110_{CoCl_2} dark-field image, figure 2(*c*), shows *continuous* moiré fringes for lengths as great as 1 μm. The fringes are somewhat wavy in nature. Allinson has shown that moiré fringes curve as they obliquely cross bend contours [11]. Hence the wavy nature of the moiré fringes is attributed to bending and local strains of the GIC crystal. The continuous nature of the fringes suggests that the crystallographic coherence length is of the order of 1 μm. If the intercalate layers consist of independent islands with sizes of the order of 500 Å, then

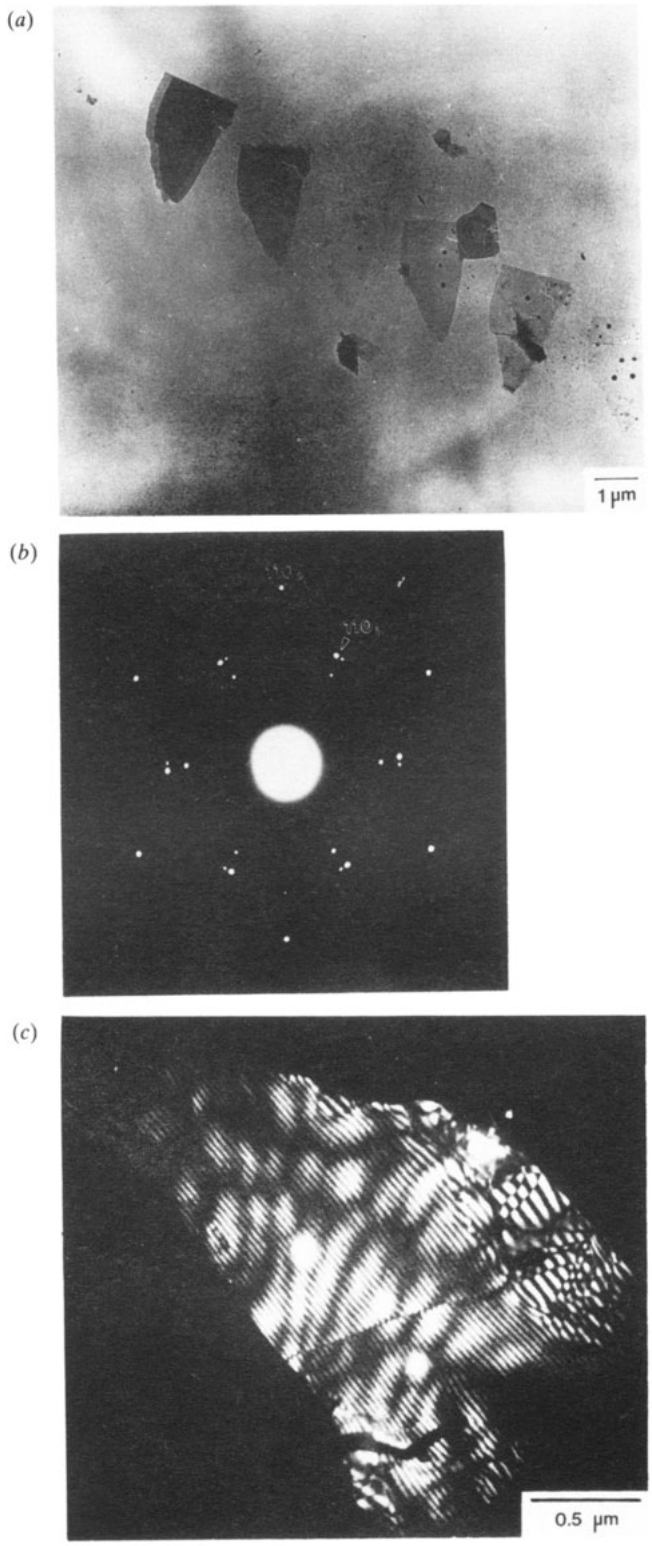

Figure 2. (*a*) Small fragments of $CoCl_2$-GIC powder. Note that the fragments are formed by repeated cleavage of a parent particle. (*b*) Selected-area diffraction pattern from a cleaved fragment showing stage 2 character (i.e., 30° rotational epitaxy angle). (*c*) 300_{CoCl_2} ($+110_{carbon}$) dark-field image from a cleaved stage 2 $CoCl_2$-GIC fragment. Note the long continuity length of the fringes.

the longest possible length for a continuous fringe would be approximately the average island size. This can be shown simply by considering the formula for the kinematic dark-field intensities in the x–y plane for two overlaying crystals which are rotated about a common axis:

$$I(\boldsymbol{r}) = \tfrac{1}{2} + \tfrac{1}{2}(\cos 2\pi)[(x/d)(\cos\delta_1 - \cos\delta_2) + (y/d)(\sin\delta_1 - \sin\delta_2) + \varphi_1 - \varphi_2] \qquad (1)$$

where $I(\boldsymbol{r})$ is the intensity in the x–y plane, d is the interplanar spacing for the reflection used to form the image, δ_1 and δ_2 are the relative rotations of the layers (in radians), and φ_1 and φ_2 are random phase shifts to account for the origin of the layers. If the intercalate exists as uncorrelated islands, then φ_1 and φ_2 should change abruptly approximately every 250 Å, and hence the position of the fringes should also change abruptly on this length scale. What we measure, however, are fringe continuity lengths of the order of 1 μm; hence this suggests that the crystallographic correlation length is

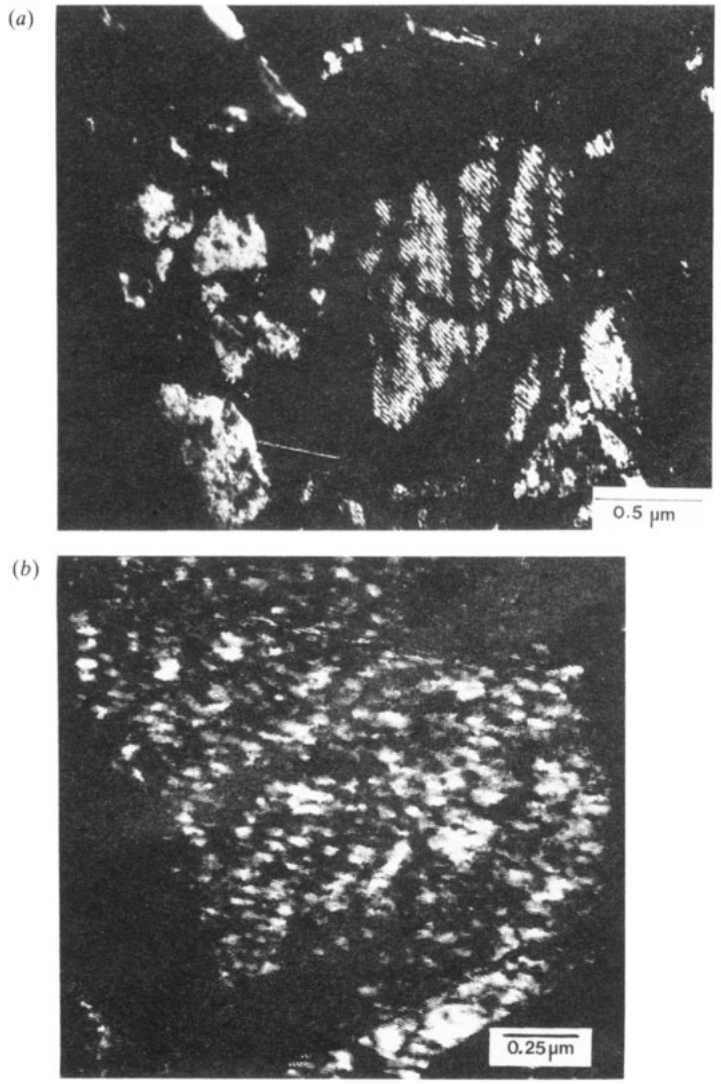

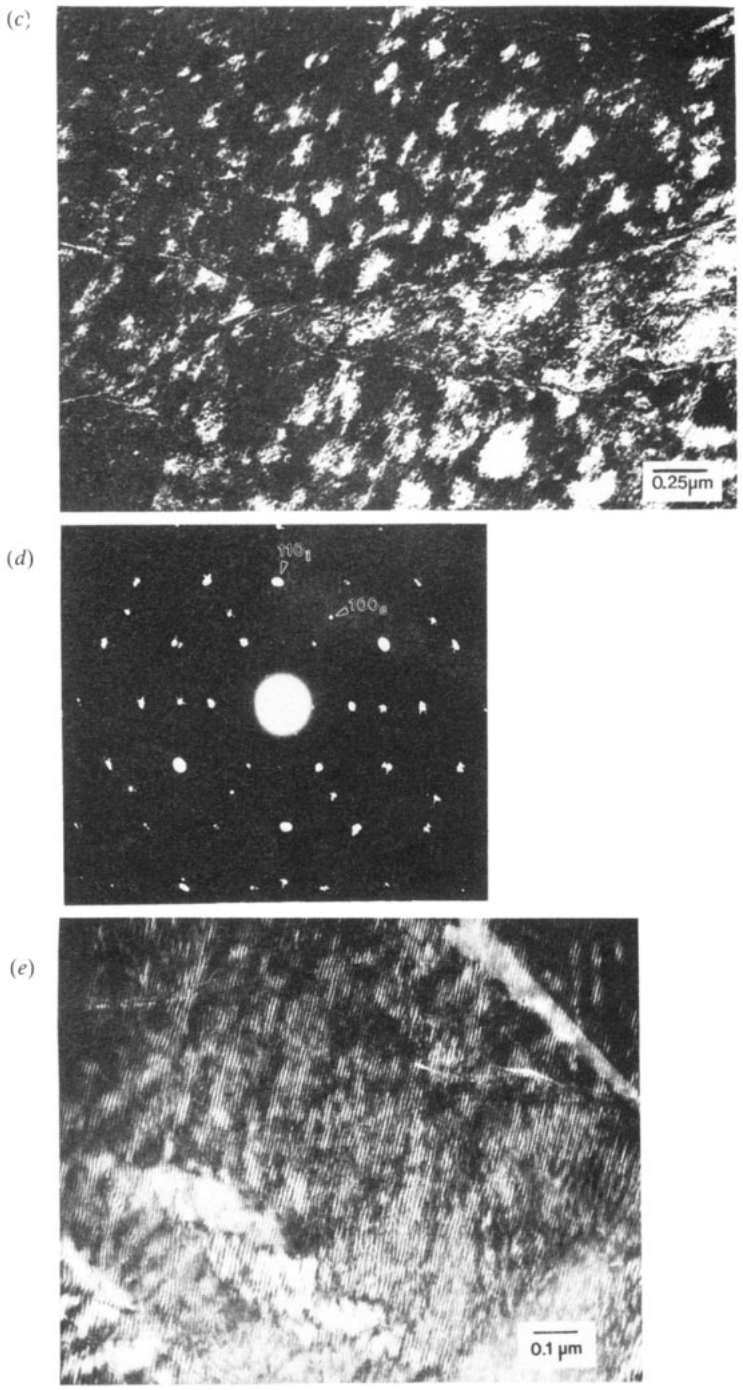

Figure 3. (*a*) 110_{CoCl_2} dark-field image from a stage 1 $CoCl_2$-GIC powder particle. Note the moiré fringe coherence length of $\simeq 0.5\,\mu m$. (*b*) 110_{CoCl_2} dark-field image of stage 1 $CoCl_2$-GIC from a natural graphite precursor; again note the moiré fringe coherence length of $\simeq 0.5\,\mu m$. (*c*) 110_{carbon} dark-field image from the same region as in (b). (d) Selected-area diffraction pattern from the same region as (*b*) and (*c*). (*e*) $hk0_{CuCl_2}$ dark-field image from stage 1 $CuCl_2$-GIC.

also of the order of 1 μm for stage 2 $CoCl_2$-GIC. The fundamental problem in the interpretation of the dark-field images from stage 2 $CoCl_2$-GIC is that a carbon ($hk0$) reflection is always close to an intercalate ($h'k'0$) reflection. Thus there is always some uncertainty over whether the moiré fringes are from the carbon or intercalate lattice. The results on stage 1 $CoCl_2$-GIC are not subject to this problem.

Similarly, in stage 1 $CoCl_2$-GIC we find regions in powder samples with moiré fringe continuity lengths of the order of 0.5 μm, as shown in figure 3(a). This is also the case for TEM samples prepared from natural graphite host materials. In figure 3(b) we show a 110_{CoCl_2} dark-field image from a sample prepared by peeling a natural graphite flake GIC. Again, fringe continuity lengths as great as $\simeq 0.5$ μm can be measured. Hence, stage 1 $CoCl_2$-GIC also has crystallographic correlation lengths of the order of 1 μm. This value is substantially larger than that determined by indirect measurements. A 110_{carbon} dark-field image is shown in figure 3(c). The patchy bright areas indicate a large local bending strain in the carbon lattice. The bending of the host layers (and hence the total

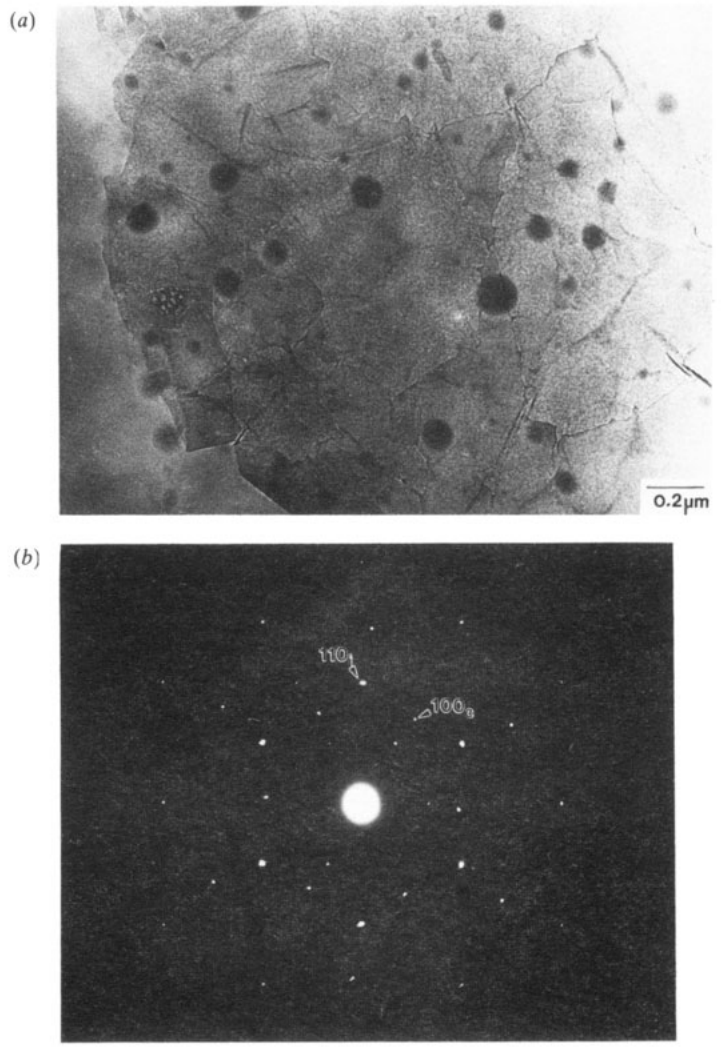

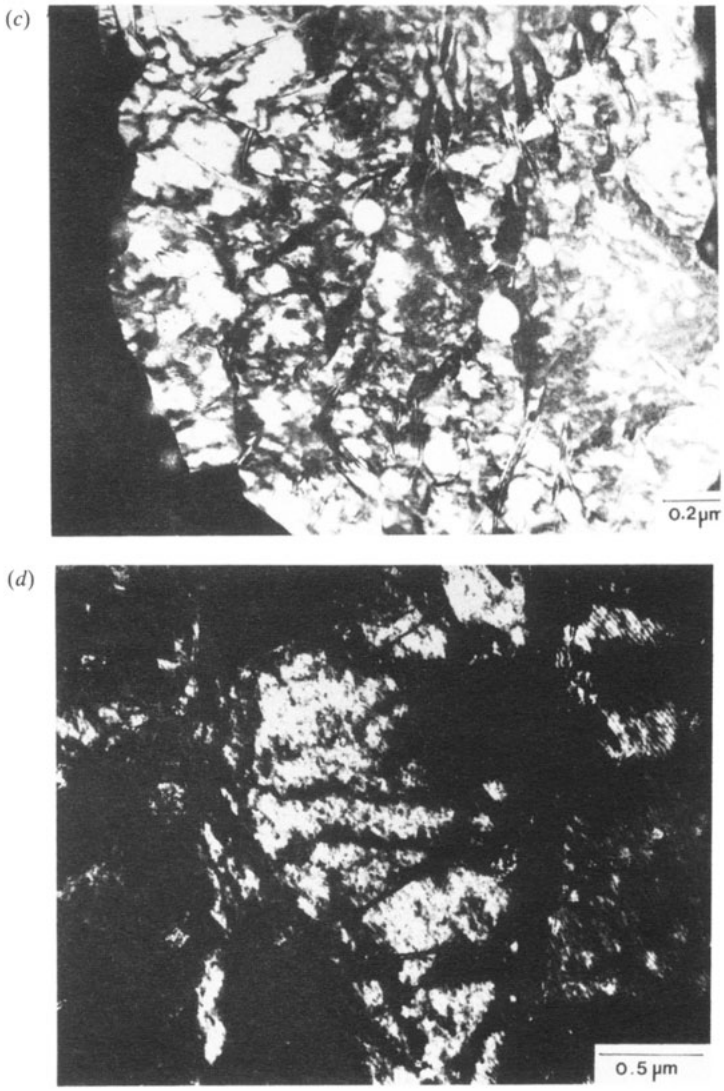

Figure 4. (*a*) Bright-field TEM image from a cleaved fragment of stage 1 $CoCl_2$-GIC. (*b*) Corresponding selected-area diffraction pattern (effective diameter of the selected-area aperture = 1.5 μm). (*c*) and (*d*) 110_{CoCl_2} dark-field images displaying long-range coherence of the intercalate layer (the dark-field image shown in (*c*) corresponds to the bright-field image shown in (*a*); the image shown in (*d*) is from a different region of the sample). The small dark circle areas (*a*) with diameters of $\simeq 0.1$ μm are contaminant particles of the free chloride. These contaminant particles appear bright in (*c*).

structure) contributes to the curved nature of the moiré fringes shown in figure 3(*b*). In figure 3(*d*) we show the selected-area diffraction pattern of the region used to form the images in figures 3(*b*) and 3(*c*). Note that there are only two intercalate orientations in this case. Similarly, we show a dark-field moiré fringe image from $CuCl_2$-GIC in figure 3(*e*). In this case it is possible to measure fringes with lengths greater than $\simeq 0.1$ μm. Again, this indicates that the crystallographic coherence length for the intercalate is of the order of 1 μm.

3.2. Metal–dichloride GICs: TEM on single domains

It is possible to find regions in powder GIC samples in which there is a single domain. The bright-field images of such regions give rise to very little contrast, as shown in figure 4(*a*). The diffraction pattern from such a region is shown in figure 4(*b*). The 0.1–0.2 μm dark regions in figure 4(*a*) are small contaminant particles of $CoCl_2$ on the specimen surface. Note that the diffraction spots for both the carbon and intercalate layers are sharp and that there is only one orientation of the intercalate layers. Imaging with the 110_{CoCl_2} reflection gives rise to images with complicated strain contrast and several bend contours as shown in figure 4(*c*) and figure 4(*d*). The important result of this experiment is that intercalate dark-field images have been obtained without moiré fringes and give direct information on the microstructure. The bend contours in figure 4(*c*) and 4(*d*) may arise from crumpling of the thin platelet. The microstructure shown in figure 4(*c*) and 4(*d*) implies that the intercalate layer in stage 1 $CoCl_2$-GIC actually exists as a complicated interconnected network. The interconnected nature of the intercalate layer gives rise to the mottled contrast in figure 4(d) which suggests lengths for continuous material of the order of 250 Å.

There are two obstacles in imaging the details of the structure of the intercalate layer. First, in order to image a single domain, we require a section perhaps 100 Å thick. The dark-field images formed from such thin sections are sufficiently weak that photographic exposure times are of the order of one minute. Such weak images are difficult to focus and it is difficult to resolve subtle variations in contrast. Second, the intercalate layer in virtually all GICs suffers considerable radiation damage, primarily radiolytic in nature, from the electron beam [12]. The beam damage effectively blurs the dark-field image.

3.3. Stage 1 $CoCl_2$-GIC: diffraction statistics and possible short-range order of defects

The statistics of the selected-area diffraction patterns provide further information on the crystallographic correlation length of the intercalate layer. In figure 5 a *c*-axis diffraction pattern of stage 1 $CoCl_2$-GIC based on a natural graphite host is shown. A 4.5 μm diameter selected-area aperture was used to form the pattern. The diffraction pattern clearly shows that there is only one discernible intercalate orientation. If the intercalate existed as isolated islands, then each island would select its own rotational epitaxy angle. Again, if an island size of 500 Å was assumed, then the intercalate in the region defined by the selected-area aperture would have $\simeq 5000$ different islands. Hence a continuous arc of reflections, with a FWHM the same as that measured by single-crystal x-ray techniques [1], would be expected for the intercalate lattice. Yet we observe discrete intercalate reflections in the diffraction patterns. Even for the diffraction pattern shown in figure 1(*a*) the reflections are still discrete, and know that there are several differently oriented layers through the thickness of the foil because of the complex moiré fringe image shown in figure 1(*b*). Based on the selected-area diffraction patterns alone, one could argue that there is a rotational coherence length separate from the crystallographic coherence length. But the rotational information must somehow be transferred from island to island. It is possible that this could take place by deformation of the host carbon layers, but the carbon is about ten times stiffer than the intercalate. Further, Wiesler has recently shown that there is little strain in the carbon layers [13]. The selected-area electron diffraction results also strongly suggest the likelihood that the crystallographic coherence length of the intercalate layer is of the order of 1 μm.

The intercalate in stage 1 $CoCl_2$-GIC stacks in a rhombohedral, $\alpha\beta\gamma$, sequence (see

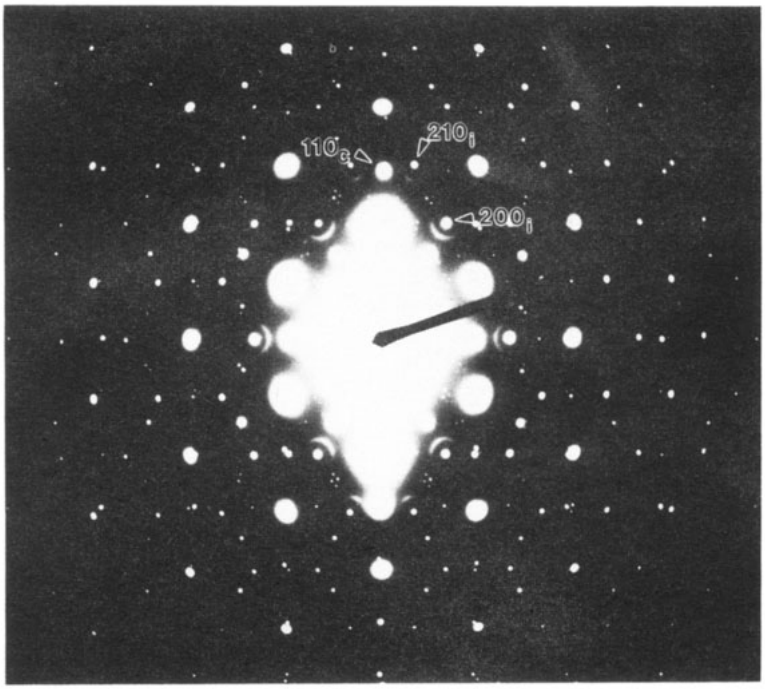

Figure 5. Selected-area diffraction pattern from stage 1 $CoCl_2$-GIC from a natural graphite flake host. Note that only one intercalate orientation is predominant. Also note the diffuse intensity around the 100, 200, 210, . . . families of reciprocal lattice points. The {100}, {200} and {210} reflections are systematically absent because of the rhombohedral stacking of the intercalate. Any intensity at these positions comes from higher-order Laue zones.

Speck *et al* [1] for details). This leads to the condition that $-h + k + l = 3n$ (where n is an integer) must be satisfied for a reflection. The $hk0$ diffraction pattern in figure 5 shows diffuse intensity around the positions of systematically absent intercalate reflections. For example, a diffuse 'half-moon' halo surrounds the 200 position. The diffracted intensity at 200 is due to reflections from higher-order Laue zones, in this case $20\bar{1}$. The diffuse intensity surrounding 200 and similar disallowed intercalate reflections (e.g., 200) is consistent with short-range order of point defects. Diffuse scattering from short-range order is characterised by maxima in intensity away from allowed reflections and periodicity in the reciprocal lattice [14]. The diffuse scattering shown in figure 5 may be associated with the non-stoichiometry of the intercalate layer.

3.4. $InCl_3$-GICs: incommensurate phases, commensurate phases and bubble formation

$InCl_3$ also forms a chlorine/metal/chlorine sandwich when intercalated into graphite. In this case the indium atoms occupy two thirds of the octahedral sites between two close-packed chlorine layers. The basal plane structure of stage 2 and stage 3 $InCl_3$-GIC has been reported to have a $\sqrt{7} \times \sqrt{7}$ R19.1° structure commensurate with the carbon host lattice (where the in-plane lattice constant of the intercalate is $\sqrt{7}a_C$, and the a axes of the two lattices are rotated by 19.1° about a common c axis) [15–17]. A projection of the $InCl_3$ trilayer sandwich structure and its relation to the carbon host lattice are shown in figures 6(a) and 6(b), respectively.

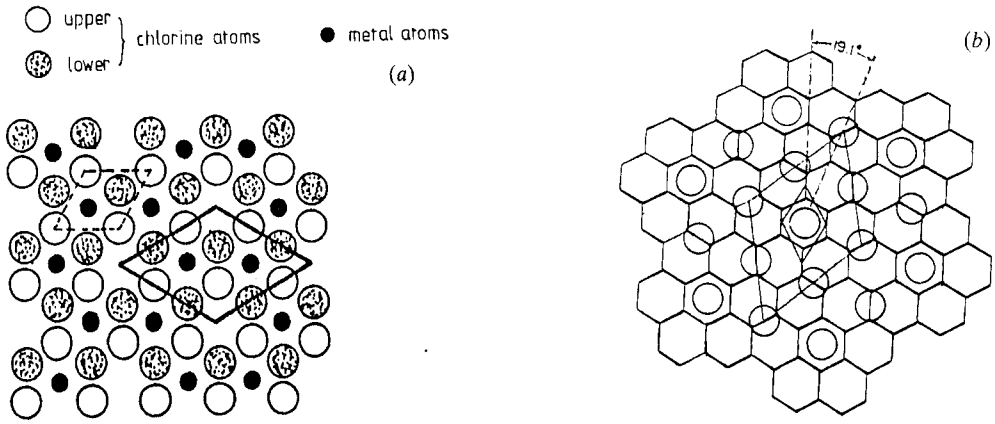

Figure 6. (*a*) *c*-axis projection of the structure of the intercalate sandwich in $InCl_3$-GIC. The unit cell drawn with dark full lines is the basal unit cell of the entire $InCl_3$ sandwich. The unit cell drawn with broken lines is the basal unit cell of an individual chlorine layer. Note that these two cells are rotated by 30° and that the length of the cell edges differ by a factor of $\sqrt{3}$. (*b*) Real space $\sqrt{7} \times \sqrt{7}$ R19.1° superlattice structure where the open circles denote the position of chlorine atoms relative to the carbon basal layer.

The $InCl_3$-GIC samples that we prepared had a crumpled appearance after the reaction. Both (00*l*) x-ray diffraction patterns and precession photographs showed only weak evidence for intercalation. This result suggests that our samples partially deintercalated on cooling in the reaction ampoule. TEM on these samples showed several regions with pure graphitic regions. Nevertheless, it was easy to find residue regions in the samples that contained $InCl_3$. A bright-field image of a residue region is shown in figure 7(*a*). The dark region in the centre of figure 7(*a*) corresponds to a structure that is nearly commensurate with the $\sqrt{7} \times \sqrt{7}$ R19.1° structure. In the following we refer to this structure as the 'nearly commensurate $\sqrt{7} \times \sqrt{7}$ R19.1° structure' and the corresponding diffraction pattern is shown in figure 7(*b*). The regions with low intercalate density, such as the peripheral regions in figure 7(*a*), correspond to an aligned incommensurate structure. The diffraction pattern for the incommensurate aligned phase is shown in figure 7(*c*). This phase has not been previously reported. The intercalate lattice constants of the aligned incommensurate phase and the nearly commensurate $\sqrt{7} \times \sqrt{7}$ R19.1° phase are the same (within the limits of uncertainty in electron diffraction), $a_{InCl_3} = 6.38$ Å.

The nearly commensurate nature of the $\sqrt{7} \times \sqrt{7}$ R19.1° structure is indicated by the fact that all of the carbon 100 reflections fall slightly inside the lines of a hexagon defined by the $InCl_3$ 300 reflections. The intercalate reciprocal lattice is $\simeq 1.8\%$ larger than the $\sqrt{7} \times \sqrt{7}$ R19.1° lattice. If we assume that the carbon in-plane lattice constant is 2.455 Å (this is the approximate value we measure for the other acceptor GICs [1]), then the *a*-axis lattice constant of the $InCl_3$ is $\simeq 0.982\sqrt{7}a_C = 6.378$ Å. Unfortunately we do not know the stage number of either the nearly commensurate or the aligned phases. We speculate that it is possible that the nearly commensurate $\sqrt{7} \times \sqrt{7}$ R19.1° lattice corresponds to stage 1 regions. This is because the stage 2 compounds have been reported to be fully commensurate with the $\sqrt{7} \times \sqrt{7}$ R19.1° structure at ambient temperature [15]. At the reaction temperature of 450 °C, the $InCl_3$ may form a fully commensurate structure; then on cooling there may be a commensurate-to-incom-

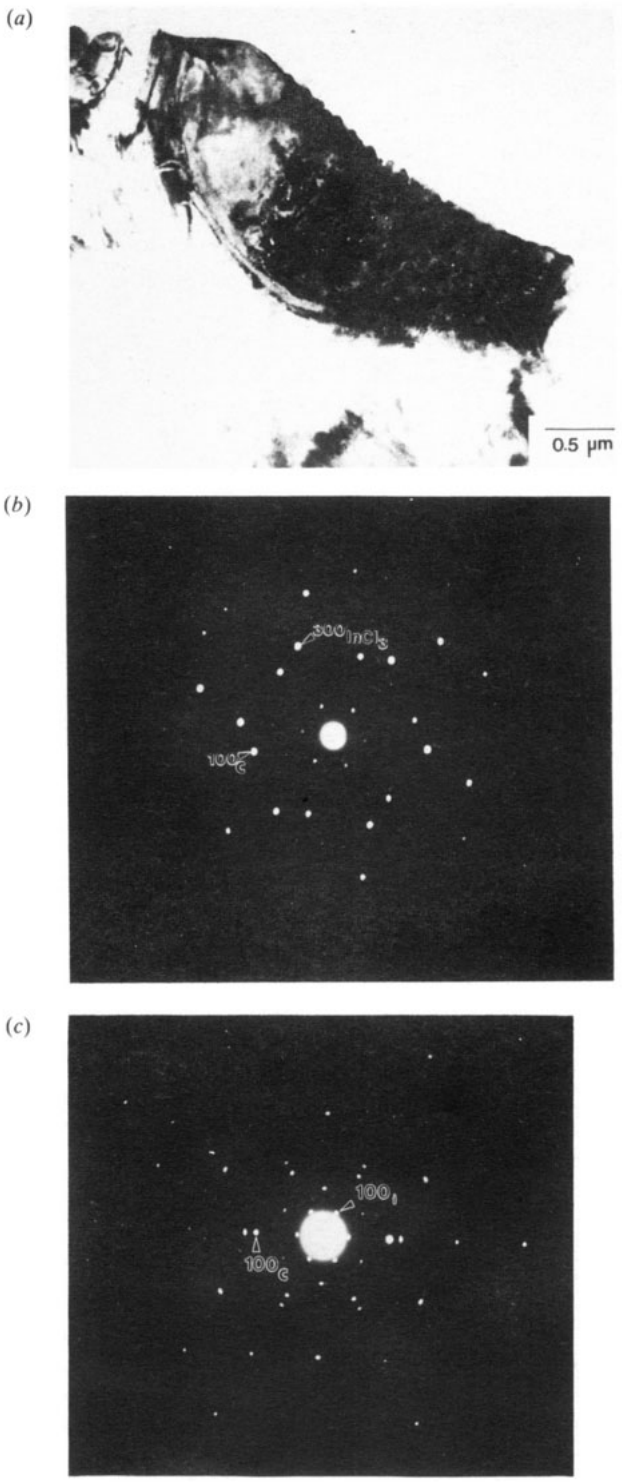

Figure 7. (*a*) Bright-field image from an $InCl_3$-GIC specimen. The dark region in the photograph has the nearly commensurate $\sqrt{7} \times \sqrt{7}$ R19.1° structure, as shown in the selected-area electron diffraction pattern in (*b*). The peripheral regions in the bright-field image shown in (*a*) have an incommensurate aligned structure, as shown in the diffraction pattern in (*c*).

mensurate (C-IC) transition because of the negative in-plane thermal expansion coefficient of carbon in this temperature range [18] and presumably a positive and larger thermal expansion coefficient for the $InCl_3$. The lattice constant of the intercalate layer is determined by a competition between the intercalate self-interaction and the intercalate–host interaction. Our results suggest that in stage 1 $InCl_3$-GIC a strong intercalate interlayer interaction drives the structure to become incommensurate, whereas in stage 2 $InCl_3$-GIC the intercalate–carbon interaction forces the structure to be commensurate.

Further insight can be gained on the nature of the aligned incommensurate phases in the metal chloride GICs if just the close-packed chlorine layer is considered. The basal unit cell of the MCl_3 is $\sqrt{3} \times \sqrt{3}$ larger than the basal unit cell of the MCl_2 lattice (figure 6(*a*)). Also the primitive basal lattice vectors of the MCl_3 are rotated 30° from those of the MCl_2 structure. If we only consider the basal lattice of a single close-packed chlorine layer, then the lattice vectors are the same for both the MCl_2 and MCl_3 structures. Hence the lattice constant for the chlorine layer of the incommensurate phase is $a_{Cl} = a_{InCl_3}/\sqrt{3} = 3.687$ Å. This value is nearly identical to that measured for the intercalate layer in $MnCl_2$-GICs [1]. Since we are considering the chlorine lattice only, the 110_{InCl_3} reflections become 100_{Cl} reflections. Hence we see that the aligned incommensurate $InCl_3$-GIC structure corresponds to a 30° rotated structure when just the chlorine lattice is considered, just as is the case for stage 2 $MnCl_2$-GIC and $CoCl_2$-GIC. This result also suggests that the aligned incommensurate phase has a stage index of 2 or greater.

High-resolution TEM micrographs of the nearly commensurate $\sqrt{7} \times \sqrt{7}$ R19.1° $InCl_3$-GIC phase show continuous lattice fringes for distances as great as $\simeq$5000 Å, an example of which is shown in figure 8. The bubble in the centre of the micrograph is due to radiation damage of the structure. There are no apparent discontinuities in the fringes.

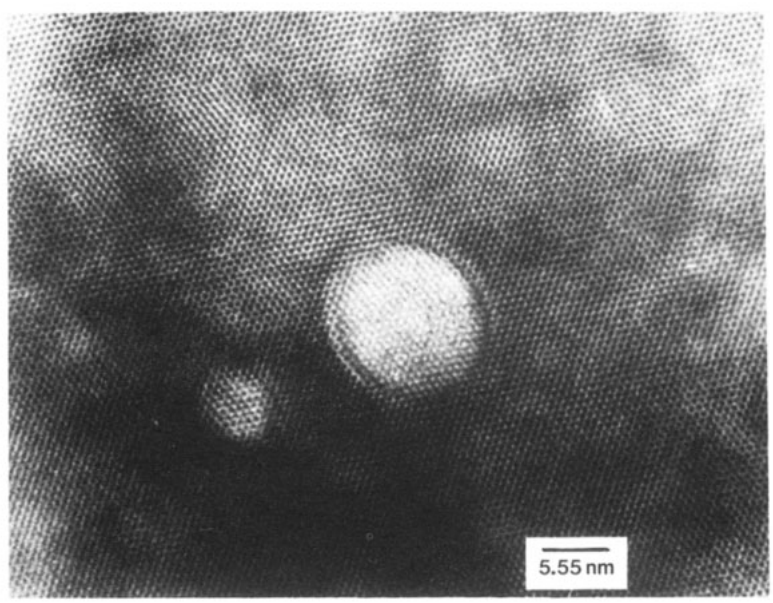

Figure 8. High-resolution micrograph of the nearly commensurate $\sqrt{7} \times \sqrt{7}$ R19.1° $InCl_3$-GIC structure. The bubble in the centre of the micrograph is due to electron beam damage of the structure.

Also there is no evidence for any incommensurate modulations in the fringe spacings. This result suggests that commensurability plays a strong role in determining the intercalate distribution. The nearly commensurate $\sqrt{7} \times \sqrt{7}$ R19.1° $InCl_3$-GIC phase has both crystallographic coherence lengths and apparent *continuity* lengths of the order of 1 μm. By continuity lengths, we refer to the average length of continuous crystal between voids or domain boundaries. In contrast, for stage 1 $CoCl_2$-GIC the dark-field intercalate micrographs suggest intercalate *continuity* lengths of the order of several hundred angströms and crystallographic coherence lengths of the order of 1 μm.

The bubble in the centre of figure 8 is due to radiolysis damage of the chloride layer. Radiolysis damage is a problem that plagues the microscopy of most insulating materials [19]. The bubbles form only under an intense electron beam. Radiation-induced bubbles have been observed in bisulphate-GICs [20]. Their rate of formation is proportional to the beam current. The bubbles have a high mobility under the electron beam. The stoichiometry of stage 2 $InCl_3$-GIC has been reported to be $C_{17.9\pm0.2}InCl_{3.6\pm0.3}$ [16]. We speculate that the bubbles are actually a Cl_2-rich fluid (with some In) which has precipitated from the chlorine-rich intercalate layer. The bubbles form, migrate, coalesce, break apart, and collapse, and then form again in an apparently chaotic fashion. This behaviour demonstrates that the electron beam induces an atomic mobility of the intercalate atoms comparable to what they have near their melting point ($\simeq$ 550 °C). There is no evidence for ring formation in the electron diffraction patterns with increasing dose rate or time. The system achieves a dynamical balance between radiation-induced damage and recovery. The intercalate layers in the $SbCl_5$-GIC system amorphise at temperatures near liquid nitrogen under the influence of the ionising electron beam [12]. As the $SbCl_5$-GIC samples are warmed to ambient temperature in the microscope (with, or without the electron beam), the intercalate layers recrystallise. The results of Salamanca-Riba *et al* [12] show that for $SbCl_5$-GIC at ambient temperature a dynamical balance is achieved between electron-beam-induced damage and recovery of the intercalate layer. At room temperature the recovery rate from beam damage to the $InCl_3$-GICs is sufficiently high that the average intercalate lattice is maintained.

The bubbles that form in this system are actually aligned columns of two-dimensional bubbles. This is because each molecular layer of intercalate is separated by at least one atomic layer of carbon. Hence for the nearly commensurate $\sqrt{7} \times \sqrt{7}$ R19.1° structure there is a strong interlayer interaction which causes the bubbles to align. Bubble formation has not been observed for the incommensurate aligned phase. If there is bubble formation in the aligned incommensurate phase, then there is no alignment of the bubbles. This result also suggests that the aligned incommensurate phase is of high stage. Below, we will show that similar effects exist for $CoCl_2$-GICs.

3.5. *STEM results: stoichiometry and bubble formation*

Bubble formation was observed in STEM analysis of stage 1 $CoCl_2$-GIC and $CuCl_2$-GICs; an example is shown in figure 9. Bubble formation in these stage 1 compounds was rarely observed in TEM observation—even after the beam had been on the sample for several minutes. This implies that the bubble formation is not dependent on the total dose, but rather on the dose rate. The alignment of the bubbles in the stage 1 compounds is driven by the intercalate interlayer interaction. The regions surrounding the bubble align to maximise the interlayer interaction, and thus reduce the free energy.

No bubble formation was observed in stage 2 $CoCl_2$-GIC or $CuCl_2$-GIC. If bubbles of a chlorine-rich fluid do form in the stage 2 compounds, then there is no observable

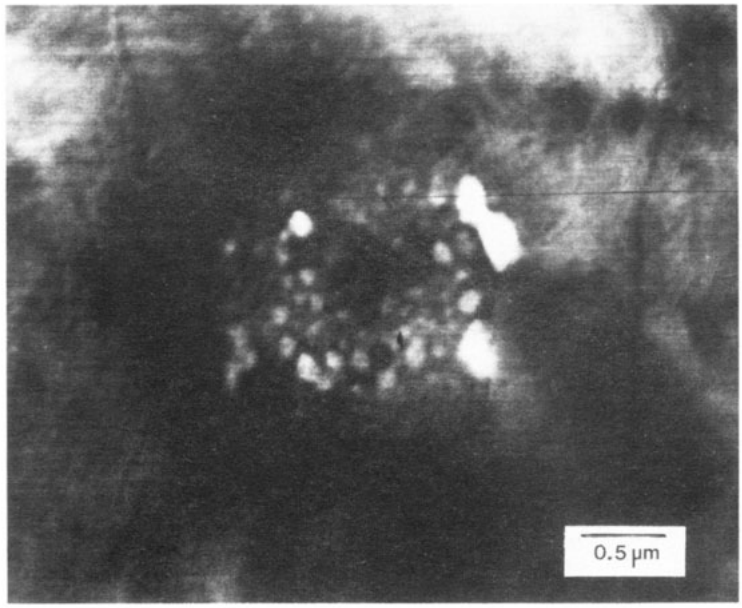

Figure 9. STEM micrograph of stage 1 $CoCl_2$-GIC showing bubble formation due to the intense localised STEM probe.

alignment of the bubbles between layers. Energy calculations for domains in stage 2 GICs show that systems with incomplete intercalate layer coverage have the lowest energy when domain walls align [21]. This is true for stage 2 systems in which the domains are on the same plane (the matching configuration) or lie on alternating planes (the staggered configuration). Both possible configurations with aligned domain walls are shown schematically in figure 10. It is possible that if bubbles form in the stage 2 compounds, they never align because the intercalate interlayer interaction is screened by the two carbon layers.

Our x-ray fluorescence measurements of the chlorine-to-metal ratio always showed a chlorine deficiency. We feel that these results are due to some radiolytic loss of chlorine during the acquisition of the x-ray fluorescence spectrum. Most measurements of the stoichiometry by wet chemical analysis show an excess of chlorine in these samples [2].

4. Discussion

4.1. Length scales for crystallographic coherence

A solid can possess several different coherence lengths. A continuous and unstrained crystal is described by a single coherence length (provided that the dimensions of the crystal are relatively uniform). An unstrained crystal with voids and pores has several different coherence lengths—at least one to describe the overall dimensions of the crystal, the crystallographic coherence length, and one or two lengths to describe the pore size and its distribution; these are the continuity lengths. These length scales are depicted schematically in figure 11 for a porous two-dimensional crystal. Small-angle neutron and x-ray scattering experiments measure discontinuities in the average scattering density. Hence a small-angle scattering experiment cannot distinguish between

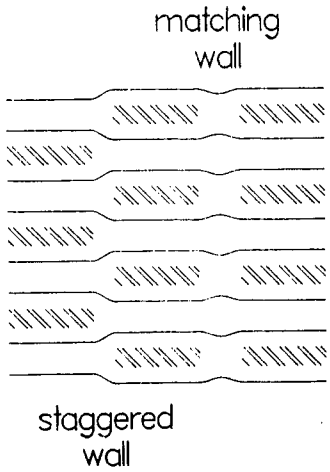

Figure 10. Matching and staggered domains in stage 2 intercalation compounds. The shaded area between the host layers represents the intercalate; the open area between the host layers represents the region where the fluid phase bubbles can be generated by the electron beam.

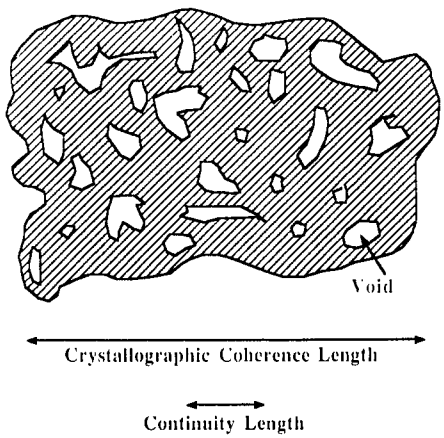

Figure 11. Schematic depiction of the crystallographic coherence length and the continuity length for a porous solid.

pores or islands. If the volume fraction of pores is small, then the linewidth of Bragg peaks is dominated by the overall dimensions of the crystal. Hence the width of a Bragg peak is a direct measure of the crystallographic coherence length of an unstrained crystal. If the crystal is inhomogeneously strained, then the Bragg peak is broadened by both crystallographic coherence effects and strain.

The results above demonstrate that the intercalate in stage 1 and stage 2 MCl_2-GICs has crystallographic coherence lengths of the order of 1 μm. The continuity length may be much smaller. The mottled appearance of the intercalate layers in single-domain dark-field micrographs, figure 4(*c*), suggests continuity lengths of the order of $\simeq$250 Å. These results show that the intercalate exists as an interconnected network, rather than as isolated islands. The exact details of the intercalate distribution are difficult to determine from TEM because of radiation damage of the intercalate layers in TEM experiments. The continuity lengths we report are entirely consistent with island sizes determined from small-angle neutron scattering measurements [6, 9]. The island sizes inferred from the widths of Bragg peaks cannot be trusted. This is because it has recently been shown that the Bragg peaks in stage 2 $CoCl_2$-GIC are strain broadened [13]. After accounting for the strain broadening of the intercalate Bragg peaks, Wiesler reported an average crystallographic coherence length of 2000 Å. This value is approximately an order of magnitude larger than that determined by other researchers [5, 6, 9]. We feel that the small-angle scattering experiments actually measure either pore size or the average length between pores or perhaps both. At this time we do not know if the pores in the intercalate layer also are contiguous.

Nicholls and Dresselhaus [22] have recently made extensive magnetic measurements on the stage 1 $CoCl_2$-GIC diluted with $MgCl_2$. They indirectly demonstrated that the $\simeq$15% concentration of voids in the intercalate gallery are distributed randomly. This

result provides further supporting evidence for our model of long-range intercalate crystallographic coherence.

4.2. The big puzzle: more pieces, but no clear picture

In this paper we have reported new data on the structure of stage 1 and stage 2 MCl_2-GICs. We will summarise our progress and shortcomings in understanding the structure.

(i) Incomplete intercalate coverage of the carbon layer. Dark-field imaging experiments on stage 1 and stage 2 $CoCl_2$-GIC demonstrate that the intercalate has crystallographic coherence lengths of the order of 1 μm and continuity lengths of the order of 250 Å. The high-resolution TEM results on the nearly commensurate $\sqrt{7} \times \sqrt{7}$ R19.1° $InCl_3$-GIC phase show that the intercalate in this case has both crystallographic coherence lengths and continuity lengths of the order of 1 μm. These two results suggest that commensurability plays a role in governing the intercalate distribution. Specifically, the a-axis lattice constant for $CoCl_2$-GIC is far from being commensurate with the graphene layers, $a_{CoCl_2}/a_{carbon} = 1.46$, so any local phase matching between the intercalate and carbon lattices is quickly lost in this case.

(ii) The other possible explanation for the incomplete intercalate coverage is in the reported chlorine excess in these compounds [2]. The diffuse haloes in the electron diffraction patterns of stage 1 $CoCl_2$-GIC suggest that there is short-range order of point defects in the intercalate layer. A slight chlorine excess in these compounds could also be considered as a slight metal deficiency. It is possible that the diffuse intensity shown in figure 5 is due to short-range order of metal vacancies. A vacancy on a metal site acts as an acceptor for electrons, hence satisfying the charge transfer requirements of the structure.

The studies reported here have expanded our knowledge of the structure of these compounds. But there still seem to be important pieces of the structural puzzle missing. We still lack a fundamental model to account for the incomplete intercalate coverage of the carbon layer in the MCl_2-GICs.

5. Conclusions

(i) An analysis of moiré fringes in dark-field TEM micrographs of stage 1 and stage 2 $CoCl_2$-GIC show that the crystallographic coherence length of the intercalate layer is of the order of 1 μm.

(ii) The statistics of selected-area electron diffraction patterns also indicate that the intercalate has crystallographic coherence lengths of the order of 1 μm.

(iii) The mottled appearance in dark-field TEM micrographs of single-intercalate-domain regions of stage $CoCl_2$-GIC suggests crystallographic continuity lengths on the order of 250 Å for the intercalate layer.

(iv) Electron diffraction results from stage 1 $CoCl_2$-GIC show diffuse intensity, characteristic of short-range order of point defects in the intercalate layer.

(v) Two new phases have been discovered in $InCl_3$-GICs: an incommensurate aligned phase, and a nearly commensurate $\sqrt{7} \times \sqrt{7}$ R19.1° phase. The nearly commensurate $\sqrt{7} \times \sqrt{7}$ R19.1° phase is believed to be associated with stage 1. The aligned phase is believed to be stage 2 or a higher stage. The nearly commensurate $\sqrt{7} \times \sqrt{7}$ R19.1° phase displays both crystallographic coherence and continuity lengths in excess of 1 μm.

(vi) X-ray fluorescence determination of the stoichiometry of stage 1 and stage 2 $CoCl_2$-GICs and $CuCl_2$-GICs shows a slight chlorine deficiency. This is contrary to other reports of the stoichiometry of these compounds. It is believed that the measured chlorine deficiency is due to radiolysis damage of the intercalate layer, and not a true chlorine deficiency in these compounds.

References

[1] Speck J S, Nicholls J T, Wuensch B J, Delgado J M, Dresselhaus M S and Miyazaki H 1990 in preparation
[2] Baron F, Flandrois S, Hauw C and Gaultier J 1982 *Solid State Commun.* **42** 759
[3] Chouteau G, Schweizer J, Tasset F and Yazami R 1988 *Synth. Met.* **23** 249
[4] Wertheim G K 1981 *Solid State Commun.* **38** 633
[5] Gaultier J, Hauw C, Masson J-M, Rouillon J-C and Flandrois S 1979 *C.R. Acad. Sci., Paris* **289** 45
[6] Simon C, Batallan F, Rosenman I, Ayache C and Bonjour E 1987 *Phys. Rev.* B **35** 5816
[7] Wiesler D G, Suzuki M and Zabel H 1987 *Phys. Rev.* B **36** 7051
[8] Wiesler D G and Zabel H 1987 *Phys. Rev.* B **36** 7303
[9] Flandrois S, Hewat A W, Hauw C and Bragg R H 1983 *Synth. Met.* **7** 305
[10] Speck J S, Delgado J M, Chen S T, Yeh N C, Dresselhaus M S and Gibson J M 1986 *Symp. on Graphite Intercalation Compounds at the Materials Research Society Meeting (Boston, MA, 1986)* ed M S Dresselhaus, G Dresselhaus and S A Solin (Pittsburgh, PA: Materials Research Society Press) extended abstracts, p 44
[11] Allinson D L 1968 *Phil. Mag.* **17** 339
[12] Salamanca-Riba L, Roth G, Gibson J M, Kortan A R, Dresselhaus G and Birgeneau R J 1986 *Phys. Rev.* **33** 2738
[13] Wiesler D G 1989 Magnetic properties of transition metal dichloride-graphite intercalation compounds *PhD Thesis* University of Illinois
[14] Warren B E 1969 *X-Ray Diffraction* (Reading, MA: Addison-Wesley) p 227
[15] Vangelisti R, Nadi N and Lelaurain M 1983 *Synth. Met.* **7** 297
[16] Nadi N E, McRae E, Maréché J F, Lelaurain M and Hérold A 1986 *Carbon* **24** 695
[17] Behrens P and Metz W 1988 *Synth. Met.* **23** 81
[18] Kelly B T 1981 *Physics of Graphite* (London: Applied Science) p 191
[19] Hobbs L W 1979 *Introduction to Analytic Electron Microscopy* ed J J Hren, J Goldstein and D Joy (New York: Plenum) p 437
[20] Edgerton R F 1979 *Modulated Structures—1979 (AIP Conf. Proc. 53)* (Kailua Kona, HI: American Institute of Physics) p 69
[21] Ulloa S E and Kirczenow G 1986 *Comment. Condens. Matter. Phys.* **12** 181
[22] Nicholls J T and Dresselhaus G 1990 *Phys. Rev.* B **41** 9744